





High-pressure II-III phase transition in solid hydrogen: Insights from state-of-the-art *ab initio* calculations

Maria Hellgren , Damian Contant , Thomas Pitts, and Michele Casula 
Sorbonne Université, MNHN, UMR CNRS 7590, IMPMC, 4 place Jussieu, 75005 Paris, France

 (Received 3 May 2022; revised 28 July 2022; accepted 24 August 2022; published 17 October 2022)

The high-pressure II-III phase transition in solid hydrogen is investigated using the random phase approximation and diffusion Monte Carlo. Good agreement between the methods is found confirming that an accurate treatment of exchange and correlation increases the transition pressure by more than 100 GPa with respect to semilocal density functional approximations. Using an optimized hybrid functional, we then reveal a low-symmetry structure for phase II generated by an out-of-plane librational instability of the $C2/c$ phase III structure. This instability weakens the in-plane polarization of $C2/c$ leading to the well-known experimental signatures of the II-III phase transition such as a sharp shift in vibron frequency, infrared activity, and lattice parameter ratio c/a . Finally, we discuss the zero-point vibrational energy that plays an important role in stabilizing phase III at lower pressures.

DOI: [10.1103/PhysRevResearch.4.L042009](https://doi.org/10.1103/PhysRevResearch.4.L042009)

The phase diagram of pure hydrogen has intrigued and challenged theoretical and experimental physicists for decades. Despite being the simplest element, high-pressure hydrogen forms complex solid phases governed by strongly interacting electrons and quantum nuclei [1–3]. Present knowledge suggests that at low pressure, hydrogen consists of freely rotating molecules centered on a hcp structure (phase I). At 110 GPa the Raman roton bands disappear [4,5], and small vibron discontinuities are observed [6]. This is the onset of the broken-symmetry phase (phase II), in which the rotational motion is hindered due to the increasing anisotropic intermolecular interactions, while maintaining strong fluctuating behavior due to the relevance of nuclear quantum effects (NQEs) [7–10]. Around 150 GPa, hydrogen enters phase III. The II-III phase transition has been the subject of several studies [11–18]. The transition is detected by the sharp drop in vibron frequency [19,20], combined with a rapid increase in infrared (IR) activity [6]. The spectral signatures are experimentally well established, and the structures are not expected to largely deviate from the hcp symmetry [21]. However, little is still known concerning the orientational order. Although several structures have been proposed based on theoretical considerations [15,22–28], large uncertainties remain since their relative energies have been difficult to accurately determine with first-principles calculations. This is not only mainly due to the approximate treatment of the electron-electron interaction [29–31], but also due to difficulties in including NQEs [32–36].

The most promising candidates for phase III are layered structures, in particular, one of $C2/c$ symmetry [37–41] and a more recent one of $P6_122$ symmetry [42,43]. The planar arrangement of the H_2 molecular units induces a polarization and stretches the H_2 bond length. This leads to the strong IR activity and the softened vibron frequency when compared with the many phase II candidate structures, which all contain canted molecules with respect to the hcp planes [15,28]. Most approximations within density functional theory (DFT) predict the static (i.e., clamped nuclei) II-III transition to occur below or around the experimental value at about 150–155 GPa [18,21]. However, more accurate diffusion Monte Carlo (DMC) [30] and coupled-cluster single-double (CCSD) [31] calculations have been shown to shift the static transition pressure beyond 250 GPa. Adding zero-point vibrational energies from DFT to the DMC enthalpies reduces this result by 20 GPa only [30]. These results either question the structures or suggest that the relative role played by the electron-electron interaction and lattice dynamical effects is not well understood.

In this Research Letter, we reexamine the II-III phase transition in solid hydrogen using state-of-the-art *ab initio* calculations based on the random phase approximation (RPA) and DMC. We discover a low-symmetry structure for phase II that is stabilized by nuclear vibrations and, unlike previous candidate structures, emerges from a continuous symmetry breaking of phase III. This rationalizes several experimental outcomes. Furthermore, we show that the transition pressure is compatible with experimental findings when accurate electronic energies are considered, together with zero-point energy variations. We finally provide an estimate of NQEs, in terms of quantum anharmonicity across the transition.

Many previous works have applied DMC to hydrogen, and it provides the gold standard for this system [29,30,44,45]. Here, we use DMC in its lattice-regularized version [46] to project an initial variational wave function of Jastrow-Slater

Published by the American Physical Society under the terms of the [Creative Commons Attribution 4.0 International license](https://creativecommons.org/licenses/by/4.0/). Further distribution of this work must maintain attribution to the author(s) and the published article's title, journal citation, and DOI.

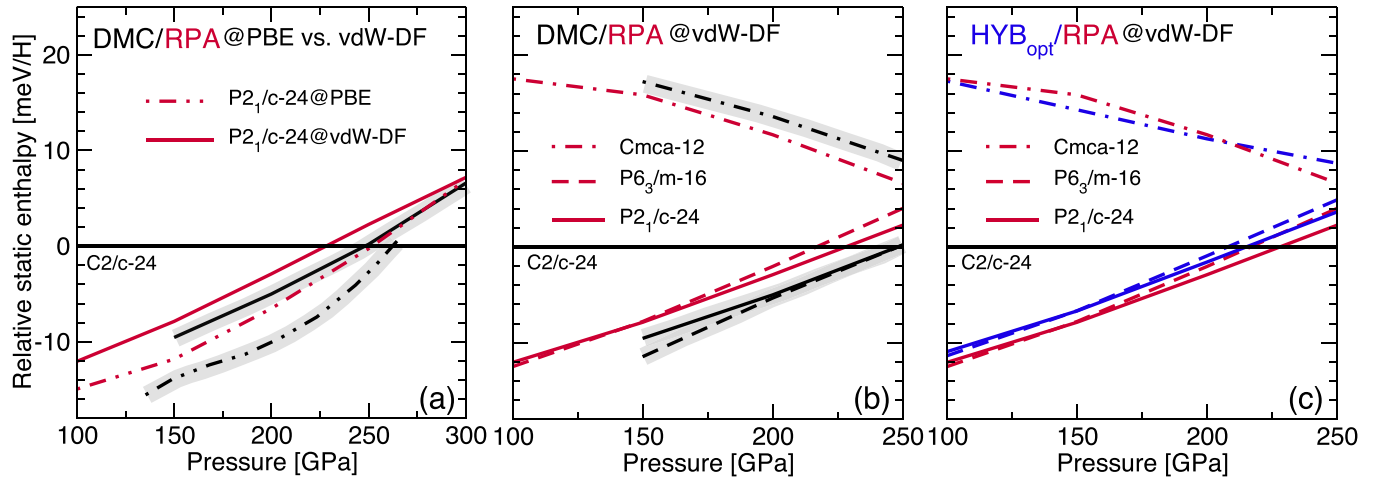


FIG. 1. RPA (red) compared with DMC (black) [(a) and (b)] and HYB_{opt} (blue) (c). The “@DFT” notation refers to the DFT approximation used to optimize the geometry at fixed pressure. The $P2_1/c-24@PBE$ result is extracted from Ref. [30]. The DMC error bars are indicated by a gray shaded area, having a height of ± 0.9 meV, around the mean values.

form, with Slater orbitals generated by DFT within the local density approximation. Further details can be found in the Supplemental Material (SM) [47].

The RPA is known for high accuracy at moderate computational cost [48–50] and is here applied to hydrogen for the first time. It combines exact exchange with a formally exact expression for the correlation energy E_c written in terms of the dynamical linear density response function χ_λ

$$E_c = - \int_0^1 d\lambda \int_0^\infty \frac{d\omega}{2\pi} \text{Tr} \{ v[\chi_\lambda(i\omega) - \chi_s(i\omega)] \}. \quad (1)$$

Within the RPA, $\chi_\lambda(i\omega)$ fulfills the time-dependent Hartree equations: $\chi_\lambda(i\omega) = \chi_s(i\omega) + \chi_s(i\omega)\lambda v \chi_\lambda(i\omega)$, where $\chi_s(i\omega)$ is the independent-particle Kohn-Sham response function and v is the Coulomb interaction. Including a vertex via the exact-exchange kernel leads to the RPA with exchange (RPAX), which has proven to give more reliable energy differences due to systematically improved total energies [51–56]. Here, we will use the RPAX, not only as an additional validation of the RPA, but also to optimize the fraction of exchange in an approximate hybrid functional.

We start by demonstrating the performance of RPA in the 100–300 GPa pressure range. We study several structures previously proposed in the literature (denoted by their symmetry and number of atoms): $P2_1/c-24$, $P6_3/m-16$, and $Pca2_1-8$ for phase II and $C2/c-24$ and $Cmca-12$ for phase III. Within a given symmetry the geometry is optimized using the van der Waals density functional (vdW-DF) [57]. Previous calculations have shown that this functional gives accurate geometries at fixed volume for molecular solid hydrogen [29]. In Fig. 1(a) we report the results for the static enthalpy difference between $P2_1/c-24$ and $C2/c-24$ with DMC and RPA, as well as the result from an earlier DMC calculation that used structures optimized with the Perdew-Burke-Ernzerhof (PBE) functional [30]. For comparison, RPA results obtained on PBE structures are also presented [58]. First of all, we see that the shift in transition pressure due to the change of functional used to optimize the geometry is of the order of 20 GPa with both DMC and RPA. Secondly, RPA is found to be in very good

agreement with DMC, staying consistently within 2 meV/H around the DMC mean value over the whole pressure range.

In Fig. 1(b), $P6_3/m-16$ and $Cmca-12$ are also included. A recent CCSD calculation of static enthalpies predicted the phase II candidate $P6_3/m-16$ to be the most stable phase up to 350 GPa [31]. Our DMC calculation contradicts this result, with $P6_3/m-16$ being degenerate with $P2_1/c-24$ within error bars (± 0.9 meV). This behavior is also confirmed by our RPA calculation, and it is independent of the theory used to optimize the geometry. There is also a good agreement between DMC and RPA for the $Cmca-12$ structure. $Cmca-12$ was originally a candidate for phase III but is now expected to become important at higher pressures, close to the insulator-to-metal transition [38–41,44,45,59].

We have also carried out RPAX calculations on the same structures. Including exchange in the response function has a very small effect on the RPA energy differences in these systems, as shown in the SM [47]. Thus the agreement between RPA, RPAX, and DMC provides strong confirmation that the static II-III transition pressure, with the currently known structures, should lie at about 225–250 GPa, irrespective of whether $P2_1/c-24$ or $P6_3/m-16$ is used for phase II. We will later show that, according to our most accurate calculations, a third competing symmetry for phase II, i.e., $Pca2_1-8$, lies very close in energy to the other two phases. These results imply an overestimation of 70–100 GPa with respect to experiment. This is also independent of whether $C2/c-24$ or $P6_122-36$ is used for phase III. Indeed, they can be considered degenerate within the DMC error bars in the pressure range analyzed here (see SM). However, we chose $C2/c-24$ as a reference structure for phase III in what follows.

To investigate the reason for the difference with respect to experiment and to include effects of lattice vibrations, we now analyze the possibility of using a hybrid functional that retains the DMC and RPA accuracy at a cheaper cost. The standard PBE0 functional with 25% of exchange does not improve the enthalpy differences with respect to semilocal DFT functionals (see SM [47]). However, exact exchange is clearly of crucial importance in the molecular phases of solid

hydrogen since PBE and Hartree-Fock alone give II-III transition pressures at 110 GPa and beyond 450 GPa, respectively [31]. We will therefore optimize a new fraction of exchange using the accurate RPax total energy. The optimization is carried out by minimizing the RPax total energy of an isolated H_2 molecule with respect to the fraction of exchange used to generate the input density [60,61]. The approach is described in Ref. [56] and in the SM [47]. We find a minimum at 48%, which is well beyond the standard value. The results from this optimized hybrid functional, which we denote as HYB_{opt} , are presented in Fig. 1(c). The good agreement with RPA shows that a hybrid functional with a carefully chosen exact-exchange fraction is sufficient to produce accurate enthalpies.

We can now use HYB_{opt} to study the stability of the structures and the impact of their relaxed geometry [62]. Comparing enthalpy differences using vdW-DF and HYB_{opt} geometries gives a difference of less than 1 meV/H. The static enthalpy differences that we have obtained with vdW-DF geometries are thus robust to further variations in the geometry. The stability of the structures can then be studied by calculating the vibrational spectra. With HYB_{opt} we are limited to Γ -point vibrations, but with vdW-DF we can study dense \mathbf{q} -point grids. We found $P2_1/c-24$ and $P6_3/m-16$ to both be stable with vdW-DF in the pressure range investigated. Interestingly, $C2/c-24$ is found to have Γ instabilities (two nearly degenerate imaginary phonons) below 215 GPa with HYB_{opt} and below 150 GPa with vdW-DF, i.e., exactly at the expected static II-III transition within the given functional. The lowest vdW-DF libron that becomes imaginary is shown as a function of pressure in Fig. 2(a). We note that a similar behavior has been observed by Raman spectroscopy [5,14,63,64], suggesting the onset of a libron instability within phase III, in proximity to the transition pressure. The unstable libron mode generates a structure with lower symmetry, in which two-thirds of the $C2/c-24$ molecules are rotated out of plane (the structures are visualized in the SM [47]). The space-group symmetry is thereby reduced to $P-1$, i.e., only inversion symmetry remains. By displacing the atoms in $C2/c-24$ according to the phonon mode eigenvector, we find a symmetric double-well potential. However, the minimum of this potential is strongly underestimated since the molecular tilting should be accompanied by an H_2 bond length contraction and an expansion of the lattice parameter ratio c/a . Indeed, after a full geometry relaxation, the energy gain increases by two orders of magnitude. Using our HYB_{opt} optimized geometries, the lowering of energy is confirmed at both the RPA and DMC levels [Fig. 2(d)].

In Fig. 2 we summarize the results for the phase diagram with clamped nuclei, including also the stable $Pca2_1-8$ phase II structure. Comparing DMC, RPA, HYB_{opt} , and vdW-DF, a clear trend emerges. The position of the instability in $C2/c-24$ coincides with the transition between $C2/c-24$ and all the proposed phase II structures, which are all nearly degenerate, independently of which functional is used. Furthermore, all approximations predict the $P-1-24$ structure to lie above the phase II candidates. Therefore $P-1-24$ does not appear competitive at any pressure. However, this picture changes when we consider lattice vibrations.

Let us now include lattice dynamics via the harmonic zero-point vibrational energy (ZPE). Due to the presence of the

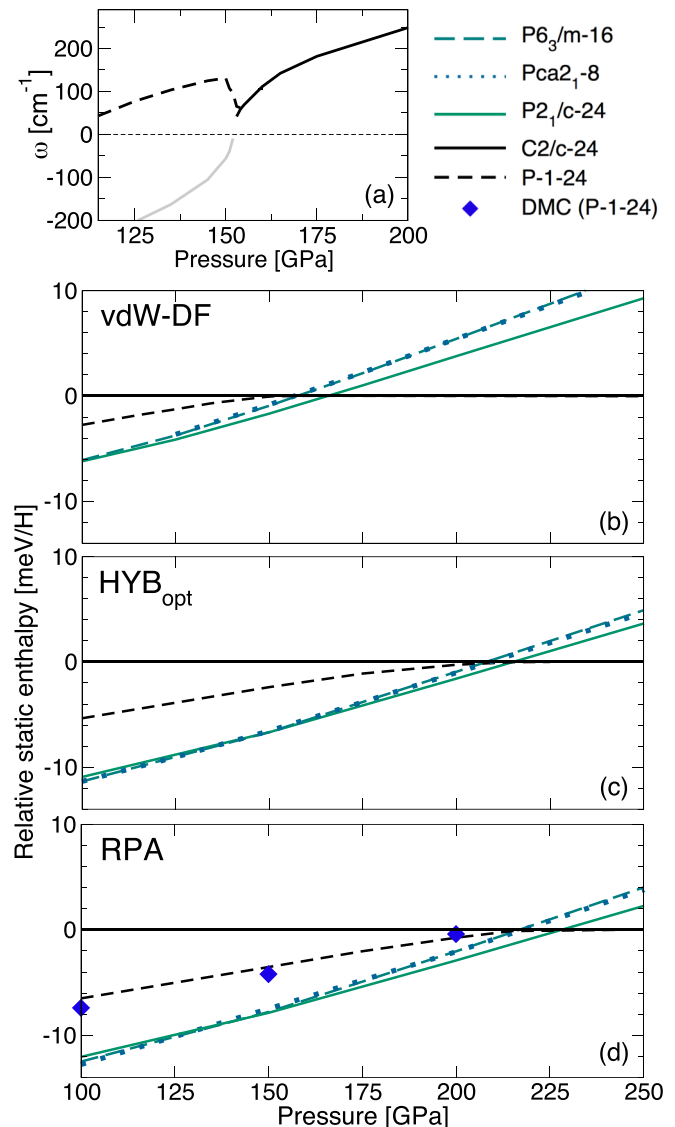


FIG. 2. The frequency of the unstable vdW-DF libron as a function of pressure is shown in (a), with the imaginary frequency (gray) shown as a negative frequency. Relative static enthalpy of $P2_1/c-24$, $P6_3/m-16$, and $Pca2_1-8$ with respect to $C2/c-24$ for (b) vdW-DF, (c) HYB_{opt} , and (d) RPA. The enthalpy of the structure obtained by following the librational instability of $C2/c-24$ is also displayed and is denoted as $P-1-24$. The DMC results for $P-1-24$ are marked with blue diamonds in (d). Their size spans the range covered by the DMC error bars.

$C2/c-24$ instability, it is necessary to use the same functional for the electronic energy as for generating the structures and computing the ZPEs. Previous calculations used PBE structures, where such an instability occurs below the range of interest (at 110 GPa) [30]. Calculating the ZPE with RPA and HYB_{opt} is presently not feasible due to the high computational cost of using supercells. However, we can consistently include the ZPE within the cheaper vdW-DF functional [65]. The result can be found in Fig. 3. We immediately see that the corresponding picture is different. The phase II candidates are all shifted by roughly the same amount, falling above the $C2/c-24$ and $P-1-24$ structures. Below 150 GPa, $P-1-24$

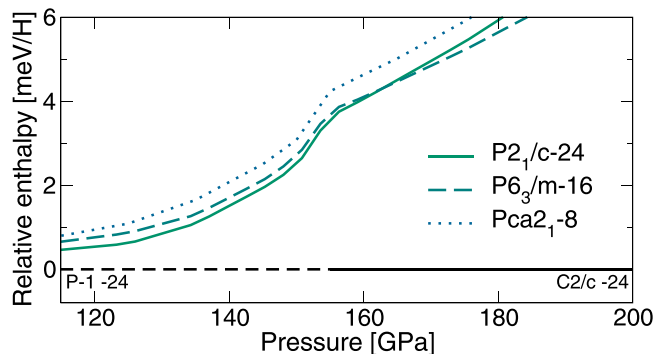


FIG. 3. Relative enthalpies within vdW-DF including ZPEs in the harmonic approximation. The ZPE of P -1-24 is smaller than the ZPE of $P2_1/c$ -24, $P6_3/m$ -16, and $Pca2_1$ -8, reversing their order of stability.

is now the most stable. Given the similarity in qualitative behavior between the different functionals, it is plausible that we would find the same ordering of enthalpies with the more advanced electronic structure methods.

Having shown that P -1-24 is a promising candidate for phase II, let us move to an in-depth analysis of the transition. A well-established experimental feature of the II-III phase transition is the sharp shift of 80 cm^{-1} in vibron frequency [19–21,59]. In Fig. 4 we plot the lowest vibron frequency, which is Raman active, as a function of pressure. Figure 4(a) shows the vdW-DF results for $C2/c$ -24, $P2_1/c$ -24, $P6_3/m$ -16, and $Pca2_1$ -8, and Fig. 4(b) shows the HYB_{opt} results for $C2/c$ -24 and $P2_1/c$ -24. The change of $C2/c$ -24 into P -1-24

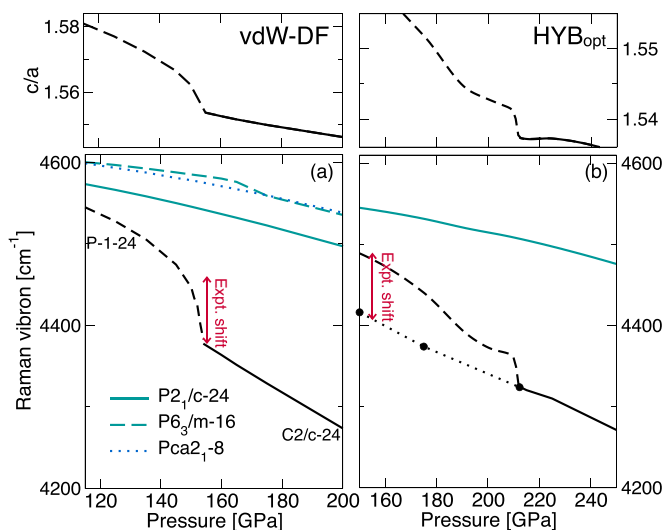


FIG. 4. (a) The lowest vibron frequency as a function of pressure within vdW-DF for $P2_1/c$ -24, $P6_3/m$ -16, $Pca2_1$ -8, and $C2/c$ -24. A rapid upshift in the frequency is observed at the transition from $C2/c$ -24 (solid line) to P -1-24 (dashed line). A similar shift is seen in the ratio c/a , as shown in the upper panel. (b) The same results with HYB_{opt} for $P2_1/c$ -24 and $C2/c$ -24. The black dots joined by the dotted line correspond to the frequencies obtained from the unstable $C2/c$ -24 structure. The experimental shift of 80 cm^{-1} at 155 GPa [20] is marked in both panels (vertically upshifted with respect to experiment).

is marked by dashed lines. At 155 GPa, i.e., at the transition to P -1-24, the $C2/c$ -24 vdW-DF vibron exhibits a continuous but sharp increase, whose size is very similar to the experimental result marked in red [20]. There is an overall difference of approximately 400 cm^{-1} with respect to experiment that can only be accounted for when calculating the vibrations beyond the harmonic approximation [41,66]. We note that the frequency shift going from $C2/c$ -24 to P -1-24 agrees better with experiment than going from $C2/c$ -24 to any of the other candidate phase II structures. We expect effects of anharmonicity to mostly cancel, but any effect would most likely increase the shift since the $C2/c$ -24 vibron is more anharmonic due to the stronger in-plane interactions. The HYB_{opt} result is qualitatively similar to the vdW-DF result, although the vibron shift appears sharper and is smaller than with vdW-DF. However, when extrapolated to 155 GPa using the unstable $C2/c$ -24 structure (i.e., when calculated at the experimental transition pressure), the shift again agrees well with experiment.

So far, $C2/c$ -24 has only been challenged by the similar $P6_122$ -36 structure [42,43]. To show that the mechanism we found is common to these phase-III types of structures, we have repeated the calculations above for $P6_122$ -36. Indeed, the vibron shift is almost identical and is caused by a librational instability very similar to the one in $C2/c$ -24. The results can be found in the SM [47]. One could reasonably assume that other energetically competitive planar structures, if found, for example, by structural searches using a functional beyond PBE, are likely to exhibit the same feature.

The cause of the abrupt change in vibron frequency is related to the shortening of the intramolecular bond lengths in P -1-24. Indeed, the out-of-plane rotation of the H_2 units weakens the in-plane intermolecular interactions that stretch the bond length. At the same time, the c parameter of the nearly hexagonal lattice abruptly increases. In the upper panels of Figs. 4(a) and 4(b) we have plotted the lattice parameter ratio c/a as a function of pressure. We observe a shift very similar to the one in vibron frequency [67]. This behavior has also been observed by x-ray diffraction [21]. In addition, by studying the charge distribution, we find that the polarization of some of the molecules reduces by a factor of 2 when rotated out of plane (see SM [47] for a Bader analysis [68,69] of the charges in $C2/c$ -24 and P -1-24). This change is reflected in the IR activity, which rapidly decreases moving from phase III to phase II [6]. In the SM we present the IR intensity as a function of pressure using the vdW-DF functional. A qualitatively good agreement with experiment is found.

Let us finally discuss the vibrational contribution to the pressure of the transition from P -1-24 to $C2/c$ -24. The exact calculation of the transition pressure, including all effects of vibrations, represents a very difficult task. Indeed, the electron-electron interaction should be described at least at the level of a hybrid functional, and lattice vibrations should be calculated beyond the harmonic approximation. However, we can make an initial estimate by calculating the variation in the harmonic ZPE due to the change in vibrons only. The 12 vibrons are only weakly \mathbf{k} dependent, so we can make the estimate at the Γ point. We find that the P -1-24 energy increases by around 2 meV/H with both vdW-DF and HYB_{opt} .

This would already lower the transition pressure by 40 GPa. Moreover, quantum anharmonicity strongly affects the orientational symmetry breaking of the molecular in-plane order. Indeed, the instability driven by the lowest librational modes can be modeled by a double-well potential, as previously mentioned. According to this simple model, derived from HYB_{opt} energies, NQEs reduce the transition pressure by an additional amount of 20 GPa, due to quantum resymmetrization effects (see SM) [70]. A very mild isotope effect is found, in accordance with experiments [16,71]. This brings the transition pressure obtained with the most advanced electronic structure methods to a value much closer to experiment, corroborating the mechanism of the transition.

In conclusion, using a combination of RPA, DMC, hybrid DFT, and vdW-DF functionals, we have provided insights into the nature of the II-III phase transition. We have revealed the existence of a libron instability in $C2/c-24$ that generates

a broken-symmetry phase when the pressure is lowered, in which two-thirds of the H_2 molecules are rotated out of plane. This relatively small orientational change is sufficient to quantitatively reproduce the experimental signatures of a sharp vibron shift and an order of magnitude increase of IR intensity, at the pressure where the system undergoes the transition into phase III.

The work was performed using high-performance computing (HPC) resources from GENCI-TGCC/CINES/IDRIS (Grants No. A0110907625 and No. A0110906493). Financial support from Emergence-Ville de Paris is acknowledged. This work was partially supported by the European Centre of Excellence in Exascale Computing TREX-Targeting Real Chemical Accuracy at the Exascale, funded by the European Union's Horizon 2020 Research and Innovation program under Grant Agreement No. 952165.

-
- [1] I. F. Silvera, The solid molecular hydrogens in the condensed phase: Fundamentals and static properties, *Rev. Mod. Phys.* **52**, 393 (1980).
- [2] H.-K. Mao and R. J. Hemley, Ultrahigh-pressure transitions in solid hydrogen, *Rev. Mod. Phys.* **66**, 671 (1994).
- [3] J. M. McMahon, M. A. Morales, C. Pierleoni, and D. M. Ceperley, The properties of hydrogen and helium under extreme conditions, *Rev. Mod. Phys.* **84**, 1607 (2012).
- [4] H. E. Lorenzana, I. F. Silvera, and K. A. Goettel, Orientational Phase Transitions in Hydrogen at Megabar Pressures, *Phys. Rev. Lett.* **64**, 1939 (1990).
- [5] A. F. Goncharov, R. J. Hemley, H.-K. Mao, and J. Shu, New High-Pressure Excitations in Parahydrogen, *Phys. Rev. Lett.* **80**, 101 (1998).
- [6] M. Hanfland, R. J. Hemley, and H.-K. Mao, Novel Infrared Vibron Absorption in Solid Hydrogen at Megabar Pressures, *Phys. Rev. Lett.* **70**, 3760 (1993).
- [7] S. Biermann, D. Hohl, and D. Marx, Quantum effects in solid hydrogen at ultra-high pressure, *Solid State Commun.* **108**, 337 (1998).
- [8] G. Geneste, M. Torrent, F. Bottin, and P. Loubeyre, Strong Isotope Effect in Phase II of Dense Solid Hydrogen and Deuterium, *Phys. Rev. Lett.* **109**, 155303 (2012).
- [9] Y. Crespo, A. Laio, G. E. Santoro, and E. Tosatti, Theory of the reentrant quantum rotational phase transition in high-pressure HD, *Phys. Rev. B* **84**, 144119 (2011).
- [10] M. P. Surh, K. J. Runge, T. W. Barbee, E. L. Pollock, and C. Mailhot, *Ab initio* calculations for solid molecular hydrogen, *Phys. Rev. B* **55**, 11330 (1997).
- [11] R. J. Hemley, Z. G. Soos, M. Hanfland, and H.-K. Mao, Charge-transfer states in dense hydrogen, *Nature (London)* **369**, 384 (1994).
- [12] I. I. Mazin and R. E. Cohen, Insulator-metal transition in solid hydrogen: Implication of electronic-structure calculations for recent experiments, *Phys. Rev. B* **52**, R8597 (1995).
- [13] L. Cui, N. H. Chen, and I. F. Silvera, Excitations, order parameters, and phase diagram of solid deuterium at megabar pressures, *Phys. Rev. B* **51**, 14987 (1995).
- [14] I. I. Mazin, R. J. Hemley, A. F. Goncharov, M. Hanfland, and H.-K. Mao, Quantum and Classical Orientational Ordering in Solid Hydrogen, *Phys. Rev. Lett.* **78**, 1066 (1997).
- [15] J. Kohanoff, S. Scandolo, S. de Gironcoli, and E. Tosatti, Dipole-Quadrupole Interactions and the Nature of Phase III of Compressed Hydrogen, *Phys. Rev. Lett.* **83**, 4097 (1999).
- [16] B. Edwards and N. W. Ashcroft, Order in dense hydrogen at low temperatures, *Proc. Natl. Acad. Sci. USA* **101**, 4013 (2004).
- [17] P. Tolédano, H. Katzke, A. F. Goncharov, and R. J. Hemley, Symmetry Breaking in Dense Solid Hydrogen: Mechanisms for the Transitions to Phase II and Phase III, *Phys. Rev. Lett.* **103**, 105301 (2009).
- [18] A. F. Goncharov, R. J. Hemley, and H.-K. Mao, Vibron frequencies of solid H_2 and D_2 to 200 GPa and implications for the P - T phase diagram, *J. Chem. Phys.* **134**, 174501 (2011).
- [19] R. J. Hemley and H. K. Mao, Phase Transition in Solid Molecular Hydrogen at Ultrahigh Pressures, *Phys. Rev. Lett.* **61**, 857 (1988).
- [20] H. E. Lorenzana, I. F. Silvera, and K. A. Goettel, Evidence for a Structural Phase Transition in Solid Hydrogen at Megabar Pressures, *Phys. Rev. Lett.* **63**, 2080 (1989).
- [21] Y. Akahama, M. Nishimura, H. Kawamura, N. Hirao, Y. Ohishi, and K. Takemura, Evidence from x-ray diffraction of orientational ordering in phase III of solid hydrogen at pressures up to 183 GPa, *Phys. Rev. B* **82**, 060101(R) (2010).
- [22] H. M. James, Orientational order in solid ortho-hydrogen. II. Hexagonal close-packed molecular lattice, *Phys. Rev.* **167**, 862 (1968).
- [23] H. Nagara and T. Nakamura, Stable Phases of Solid Hydrogen at Megabar Pressures and at Zero Temperature, *Phys. Rev. Lett.* **68**, 2468 (1992).
- [24] V. Natoli, R. M. Martin, and D. Ceperley, Crystal Structure of Molecular Hydrogen at High Pressure, *Phys. Rev. Lett.* **74**, 1601 (1995).
- [25] J. Kohanoff, S. Scandolo, G. L. Chiarotti, and E. Tosatti, Solid Molecular Hydrogen: The Broken Symmetry Phase, *Phys. Rev. Lett.* **78**, 2783 (1997).

- [26] K. A. Johnson and N. W. Ashcroft, Structure and bandgap closure in dense hydrogen, *Nature (London)* **403**, 632 (2000).
- [27] J. S. Tse, D. D. Klug, Y. Yao, Y. Le Page, and J. R. Rodgers, Structure and spectroscopic properties of dense solid hydrogen at 160 GPa, *Solid State Commun.* **145**, 5 (2008).
- [28] V. Labet, R. Hoffmann, and N. W. Ashcroft, A fresh look at dense hydrogen under pressure. III. Two competing effects and the resulting intra-molecular H-H separation in solid hydrogen under pressure, *J. Chem. Phys.* **136**, 074503 (2012).
- [29] R. C. Clay, J. Mcminis, J. M. McMahon, C. Pierleoni, D. M. Ceperley, and M. A. Morales, Benchmarking exchange-correlation functionals for hydrogen at high pressures using quantum Monte Carlo, *Phys. Rev. B* **89**, 184106 (2014).
- [30] N. D. Drummond, B. Monserrat, J. H. Lloyd-Williams, P. L. Ríos, C. J. Pickard, and R. J. Needs, Quantum Monte Carlo study of the phase diagram of solid molecular hydrogen at extreme pressures, *Nat. Commun.* **6**, 7794 (2015).
- [31] K. Liao, X.-Z. Li, A. Alavi, and A. Grüneis, A comparative study using state-of-the-art electronic structure theories on solid hydrogen phases under high pressures, *npj Comput. Mater.* **5**, 110 (2019).
- [32] B. Monserrat, N. D. Drummond, and R. J. Needs, Anharmonic vibrational properties in periodic systems: energy, electron-phonon coupling, and stress, *Phys. Rev. B* **87**, 144302 (2013).
- [33] S. Azadi, N. D. Drummond, and W. M. C. Foulkes, Nature of the metallization transition in solid hydrogen, *Phys. Rev. B* **95**, 035142 (2017).
- [34] G. Rillo, M. A. Morales, D. M. Ceperley, and C. Pierleoni, Coupled electron-ion Monte Carlo simulation of hydrogen molecular crystals, *J. Chem. Phys.* **148**, 102314 (2018).
- [35] L. Monacelli, R. Bianco, M. Cherubini, M. Calandra, I. Errea, and F. Mauri, The stochastic self-consistent harmonic approximation: calculating vibrational properties of materials with full quantum and anharmonic effects, *J. Phys.: Condens. Matter* **33**, 363001 (2021).
- [36] T. Morresi, L. Paulatto, R. Vuilleumier, and M. Casula, Probing anharmonic phonons by quantum correlators: A path integral approach, *J. Chem. Phys.* **154**, 224108 (2021).
- [37] C. J. Pickard and R. J. Needs, Structure of phase III of solid hydrogen, *Nat. Phys.* **3**, 473 (2007).
- [38] M. I. Eremets, A. P. Drozdov, P. P. Kong, and H. Wang, Semimetallic molecular hydrogen at pressure above 350 GPa, *Nat. Phys.* **15**, 1246 (2019).
- [39] P. Loubeyre, F. Occelli, and P. Dumas, Synchrotron infrared spectroscopic evidence of the probable transition to metal hydrogen, *Nature (London)* **577**, 631 (2020).
- [40] V. Gorelov, M. Holzmann, D. M. Ceperley, and C. Pierleoni, Energy Gap Closure of Crystalline Molecular Hydrogen with Pressure, *Phys. Rev. Lett.* **124**, 116401 (2020).
- [41] L. Monacelli, I. Errea, M. Calandra, and F. Mauri, Black metal hydrogen above 360GPa driven by proton quantum fluctuations, *Nat. Phys.* **17**, 63 (2021).
- [42] B. Monserrat, R. J. Needs, E. Gregoryanz, and C. J. Pickard, Hexagonal structure of phase III of solid hydrogen, *Phys. Rev. B* **94**, 134101 (2016).
- [43] S. Azadi and T. D. Kühne, Unconventional phase III of high-pressure solid hydrogen, *Phys. Rev. B* **100**, 155103 (2019).
- [44] J. McMinis, R. C. Clay, D. Lee, and M. A. Morales, Molecular to Atomic Phase Transition in Hydrogen under High Pressure, *Phys. Rev. Lett.* **114**, 105305 (2015).
- [45] L. Monacelli, M. Casula, K. Nakano, S. Sorella, and F. Mauri, Quantum phase diagram of high-pressure hydrogen, [arXiv:2202.05740](https://arxiv.org/abs/2202.05740).
- [46] M. Casula, C. Filippi, and S. Sorella, Diffusion Monte Carlo Method with Lattice Regularization, *Phys. Rev. Lett.* **95**, 100201 (2005).
- [47] See Supplemental Material at <http://link.aps.org/supplemental/10.1103/PhysRevResearch.4.L042009> for additional information about the computational details, structural visualization, a complementary analysis of the $P6_122-36$ structure, the nuclear quantum effects analysis across the II-III phase transition, Bader charge analysis, and infrared spectra [31,46,72–76].
- [48] X. Ren, P. Rinke, C. Joas, and M. Scheffler, Random-phase approximation and its applications in computational chemistry and materials science, *J. Mater. Sci.* **47**, 7447 (2012).
- [49] H.-V. Nguyen and S. de Gironcoli, Efficient calculation of exact exchange and RPA correlation energies in the adiabatic-connection fluctuation-dissipation theory, *Phys. Rev. B* **79**, 205114 (2009).
- [50] J. Harl and G. Kresse, Accurate Bulk Properties from Approximate Many-Body Techniques, *Phys. Rev. Lett.* **103**, 056401 (2009).
- [51] M. Hellgren and U. von Barth, Correlation energy functional and potential from time-dependent exact-exchange theory, *J. Chem. Phys.* **132**, 044101 (2010).
- [52] A. Heßelmann and A. Görling, Random phase approximation correlation energies with exact Kohn-Sham exchange, *Mol. Phys.* **108**, 359 (2010).
- [53] N. Colonna, M. Hellgren, and S. de Gironcoli, Correlation energy within exact-exchange adiabatic connection fluctuation-dissipation theory: Systematic development and simple approximations, *Phys. Rev. B* **90**, 125150 (2014).
- [54] P. Bleiziffer, M. Krug, and A. Görling, Self-consistent Kohn-Sham method based on the adiabatic-connection fluctuation-dissipation theorem and the exact-exchange kernel, *J. Chem. Phys.* **142**, 244108 (2015).
- [55] M. Hellgren, N. Colonna, and S. de Gironcoli, Beyond the random phase approximation with a local exchange vertex, *Phys. Rev. B* **98**, 045117 (2018).
- [56] M. Hellgren and L. Baguet, Random phase approximation with exchange for an accurate description of crystalline polymorphism, *Phys. Rev. Res.* **3**, 033263 (2021).
- [57] M. Dion, H. Rydberg, E. Schröder, D. C. Langreth, and B. I. Lundqvist, Van der Waals Density Functional for General Geometries, *Phys. Rev. Lett.* **92**, 246401 (2004).
- [58] All calculations are done with the QUANTUM ESPRESSO package [77] using an optimized norm-conserving Vanderbilt (ONCV) pseudopotential [78]. More details can be found in the SM.
- [59] P. Loubeyre, F. Occelli, and R. LeToullec, Optical studies of solid hydrogen to 320GPa and evidence for black hydrogen, *Nature (London)* **416**, 613 (2002).
- [60] M. Hellgren, L. Baguet, M. Calandra, F. Mauri, and L. Wirtz, Electronic structure of TiSe_2 from a quasi-self-consistent G_0W_0 approach, *Phys. Rev. B* **103**, 075101 (2021).
- [61] N. L. Nguyen, N. Colonna, and S. de Gironcoli, *Ab initio* self-consistent total-energy calculations within the EXX/RPA formalism, *Phys. Rev. B* **90**, 045138 (2014).
- [62] Structural relaxation with hybrid functionals was performed using the Vienna *ab initio* simulation package (VASP) code [79–81].

- [63] R. J. Hemley, H. K. Mao, and J. F. Shu, Low-Frequency Vibrational Dynamics and Structure of Hydrogen at Megabar Pressures, *Phys. Rev. Lett.* **65**, 2670 (1990).
- [64] A. F. Goncharov, E. Gregoryanz, R. J. Hemley, and H.-K. Mao, Spectroscopic studies of the vibrational and electronic properties of solid hydrogen to 285 GPa, *Proc. Natl. Acad. Sci. USA* **98**, 14234 (2001).
- [65] Zero-point energies are calculated using density functional perturbation theory as implemented within the QE PHONON code [77,82].
- [66] T. Morresi, R. Vuilleumier, and M. Casula, Hydrogen phase-IV characterization by full account of quantum anharmonicity, *Phys. Rev. B* **106**, 054109 (2022).
- [67] H. Kitamura, S. Tsuneyuki, T. Ogitsu, and T. Miyake, Quantum distribution of protons in solid molecular hydrogen at megabar pressures, *Nature (London)* **404**, 259 (2000).
- [68] R. F. W. Bader, A quantum theory of molecular structure and its applications, *Chem. Rev.* **91**, 893 (1991).
- [69] G. Henkelman, A. Arnaldsson, and H. Jonsson, A fast and robust algorithm for Bader decomposition of charge density, *Comput. Mater. Sci.* **36**, 354 (2006).
- [70] I. Errea, M. Calandra, C. J. Pickard, J. R. Nelson, R. J. Needs, Y. Li, H. Liu, Y. Zhang, Y. Ma, and F. Mauri, Quantum hydrogen-bond symmetrization in the superconducting hydrogen sulfide system, *Nature (London)* **532**, 81 (2016).
- [71] A. F. Goncharov, I. I. Mazin, J. H. Eggert, R. J. Hemley, and H.-K. Mao, Invariant Points and Phase Transitions in Deuterium at Megabar Pressures, *Phys. Rev. Lett.* **75**, 2514 (1995).
- [72] K. Nakano, C. Attaccalite, M. Barborini, L. Capriotti, M. Casula, E. Coccia, M. Dagrada, C. Genovese, Y. Luo, G. Mazzola, A. Zen, and S. Sorella, TURBORVB: A many-body toolkit for *ab initio* electronic simulations by quantum Monte Carlo, *J. Chem. Phys.* **152**, 204121 (2020).
- [73] S. Sorella, N. Devaux, M. Dagrada, G. Mazzola, and M. Casula, Geminal embedding scheme for optimal atomic basis set construction in correlated calculations, *J. Chem. Phys.* **143**, 244112 (2015).
- [74] C. J. Umrigar, J. Toulouse, C. Filippi, S. Sorella, and R. G. Hennig, Alleviation of the Fermion-Sign Problem by Optimization of Many-Body Wave Functions, *Phys. Rev. Lett.* **98**, 110201 (2007).
- [75] M. Calandra Buonaura and S. Sorella, Numerical study of the two-dimensional Heisenberg model using a Green function Monte Carlo technique with a fixed number of walkers, *Phys. Rev. B* **57**, 11446 (1998).
- [76] H. Kwee, S. Zhang, and H. Krakauer, Finite-Size Correction in Many-Body Electronic Structure Calculations, *Phys. Rev. Lett.* **100**, 126404 (2008).
- [77] P. Giannozzi, O. Andreussi, T. Brumme, O. Bunau, M. Buongiorno Nardelli, M. Calandra, R. Car, C. Cavazzoni, D. Ceresoli, M. Cococcioni, N. Colonna, I. Carnimeo, A. Dal Corso, S. de Gironcoli, P. Delugas, R. A. DiStasio Jr., A. Ferretti, A. Floris, G. Fratesi, G. Fugallo *et al.*, Advanced capabilities for materials modeling with Quantum ESPRESSO, *J. Phys.: Condens. Matter* **29**, 465901 (2017).
- [78] D. R. Hamann, Optimized norm-conserving Vanderbilt pseudopotentials, *Phys. Rev. B* **88**, 085117 (2013).
- [79] G. Kresse and J. Furthmüller, Efficient iterative schemes for *ab initio* total-energy calculations using a plane-wave basis set, *Phys. Rev. B* **54**, 11169 (1996).
- [80] G. Kresse and J. Furthmüller, Efficiency of *ab-initio* total energy calculations for metals and semiconductors using a plane-wave basis set, *Comput. Mater. Sci.* **6**, 15 (1996).
- [81] G. Kresse and D. Joubert, From ultrasoft pseudopotentials to the projector augmented-wave method, *Phys. Rev. B* **59**, 1758 (1999).
- [82] S. Baroni, S. de Gironcoli, A. Dal Corso, and P. Giannozzi, Phonons and related crystal properties from density-functional perturbation theory, *Rev. Mod. Phys.* **73**, 515 (2001).